

## Molecular-Based Electronically Switchable Tunnel Junction Devices

C. Patrick Collier, Jan O. Jeppesen, Yi Luo, Julie Perkins, Eric W. Wong, James R. Heath,\* and J. Fraser Stoddart\*

Contribution from the California NanoSystems Institute and the Department of Chemistry and Biochemistry, University of California, Los Angeles, 607 Charles E. Young Drive East, Los Angeles, California 90095-1569

Received June 12, 2001

**Abstract:** Solid-state tunnel junction devices were fabricated from Langmuir Blodgett molecular monolayers of a bistable [2]catenane, a bistable [2]pseudorotaxane, and a single-station [2]rotaxane. All devices exhibited a (noncapacitive) hysteretic current–voltage response that switched the device between high- and low-conductivity states, although control devices exhibited no such response. Correlations between the structure and solution-phase dynamics of the molecular and supramolecular systems, the crystallographic domain structure of the monolayer film, and the room-temperature device performance characteristics are reported.

## Introduction

Molecular electronics-based solid-state switches have been proposed as the active components in either nonvolatile random access memory circuits<sup>1</sup> or as the configurable bits for a custom-configurable logic-based computing machine.<sup>2</sup> The basis of such a device is a two-terminal molecular tunnel junction that can be electrically switched between high- and low-conductivity states. If the active device characteristics (i.e., the switching mechanism, the device volatility, the conductance of the device in its various states, etc.) arise from intrinsic molecular properties, then rational design of the switching molecule can be employed to optimize the switching characteristics. Furthermore, such molecular electronics devices should, in principle, exhibit a self-similarity with respect to device performance parameters, even as the devices are scaled to molecular dimensions.<sup>3</sup>

The development of a working model for correlating molecular structure/device property relationships represents a formidable challenge.<sup>4</sup> For example, there has yet to be demonstrated a common analytical tool that can be used to correlate the structure and dynamics of molecules in either the solution-phase or as thin films, with the characteristics of solid-state molecular electronic devices. Thus, only through systematic investigation of how device performance is modified through molecular structure variations can one hope to begin piecing such a model together. We have been investigating molecular mechanical and supramolecular complexes from the classes of compounds<sup>5</sup> known as catenanes, rotaxanes, and pseudorotaxanes as potential

candidates for solid-state molecular switch devices. These molecules and supermolecules present many advantages for such a study. First, electrochemically addressable (solution-phase) bistability can be designed<sup>6</sup> into these molecules (supermolecules), and this bistability can be thoroughly characterized using various optical and NMR spectroscopies.<sup>7</sup> Second, the catenane and rotaxane structures and pseudorotaxane superstructure can be employed as different (supra)molecular architectures for supporting similar molecular switching mechanisms. Third, the chemistry of these systems is sufficiently flexible so that amphiphilic character can be either directly, or indirectly, incorporated into their (super)structures. This property allows for the preparation of molecular monolayer Langmuir Blodgett (LB) films that can subsequently be incorporated into devices.

In this contribution, we report on solid-state devices fabricated from a bistable [2]catenane,<sup>8</sup> a bistable [2]pseudorotaxane,<sup>4</sup> and a single-station [2]rotaxane<sup>9</sup> (Figure 1). Molecular electronics switches fabricated from the [2]catenane were previously reported,<sup>1</sup> and those devices are discussed more fully here. The syntheses of the [2]pseudorotaxane and the single-station [2]rotaxane are described in this paper. All (super)molecules were prepared as LB films for incorporation into solid-state devices. Brewster angle microscopy (BAM), as well as various scanning probe microscopies, were utilized to interrogate the structure of the LB films. Remnant response curves, device cycling, device volatility, and current–voltage traces were recorded for the various solid-state devices, and those responses are correlated with the structure of the (super)molecular switches.

## Results and Discussion

**Synthesis and Characterization.** The synthesis of the [2]-catenane **1**<sup>4+</sup> has already been reported.<sup>8</sup> Here, we will describe

\* Correspondence address: Dr. James R. Heath, Department of Chemistry and Biochemistry, UCLA, 607 Charles E. Young Drive East, Los Angeles CA 90095-1569. E-mail: heath@chem.ucla.edu.

(1) Collier, C. P.; Mattersteig, G.; Wong, E. W.; Luo, Y.; Sampaio, J.; Raymo, F. M.; Stoddart, J. F.; Heath, J. R. *Science* **2000**, *289*, 1172–1175.

(2) Heath, J. R.; Keukes, P. J.; Snider, G.; Williams, R. S. *Science* **1998**, *280*, 1716–1721.

(3) Reed, M. A.; Zhou, C.; Muller, C. J.; Burgin, T. P. *Science* **1997**, *278*, 252–254.

(4) Pease, A. R.; Jeppesen, J. O.; Stoddart, J. F.; Luo, Y.; Collier, C. P.; Heath, J. R. *Acc. Chem. Res.* **2001**, *36*, 433–444.

(5) (a) Amabilino, D.; Stoddart, J. F. *Chem. Rev.* **1995**, *95*, 2725–2828. (b) Raymo, F. M.; Stoddart, J. F. *Chem. Rev.* **1999**, *99*, 1643–1663. (c) Lindoy, L. F.; Atkinson, I. M. *Self-Assembly in Supramolecular Systems*; Stoddart, J. F., Ed.; Royal Society of Chemistry: London, 2000.

(6) Balzani, V.; Credi, A.; Raymo, F. M.; Stoddart, J. F. *Angew. Chem., Int. Ed.* **2000**, *39*, 3349–3391.

(7) Ashton, P. R.; Ballardini, R.; Balzani, V.; Credi, A.; Dress, K. R.; Ishow, E.; Kleverlaan, C. J.; Kocian, O.; Preece, J. A.; Spencer, N.; Stoddart, J. F.; Venturi, M.; Wenger, S. *Chem. Eur. J.* **2000**, *6*, 3558–3574.

(8) Balzani, V.; Credi, A.; Mattersteig, G.; Matthews, O. A.; Raymo, F. M.; Stoddart, J. F.; Venturi, M.; White, A. J. P.; Williams, D. J. *J. Org. Chem.* **2000**, *65*, 1924–1936.

(9) Jeppesen, J. O.; Perkins, J.; Becher, J.; Stoddart, J. F. *Org. Lett.* **2000**, *2*, 3547–3550.

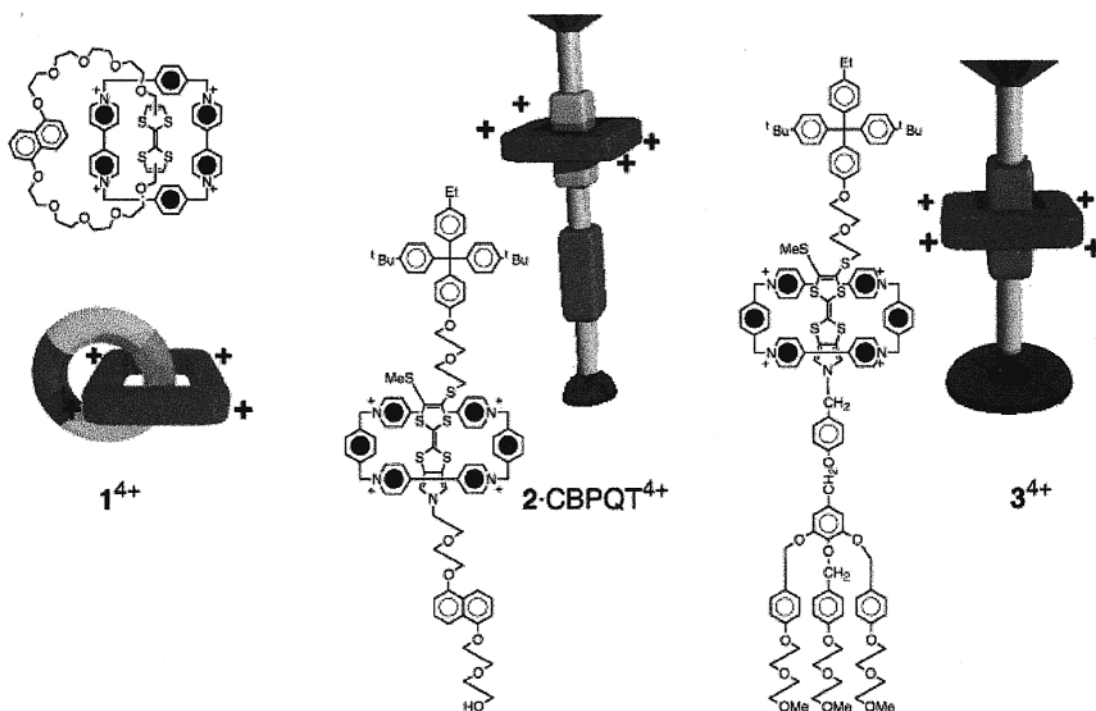


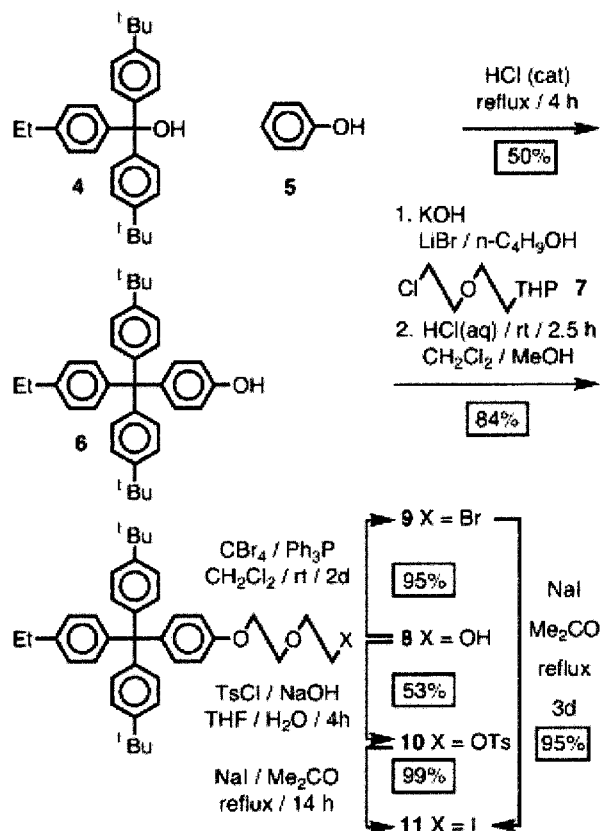
**Figure 1.** Molecular formulas and graphical representations of the [2]catenane **1<sup>4+</sup>**, the two station [2]pseudorotaxane **2·CBPQT<sup>4+</sup>**, and the single-station [2]rotaxane **3<sup>4+</sup>**.

the preparation of a hydrophobic, and also a hydrophilic, stopper before outlining the syntheses of the single-station [2]rotaxane **3<sup>4+</sup>**, incorporating both stoppers, and the two-station [2]pseudorotaxane **2·CBPQT<sup>4+</sup>** where the semidumbbell component contains only the hydrophobic stopper. Molecular formulas and graphical representations of the [2]catenane **1<sup>4+</sup>**, the two-station [2]pseudorotaxane **2·CBPQT<sup>4+</sup>**, and the single-station [2]rotaxane **3<sup>4+</sup>** are shown in Figure 1.

The hydrophobic tetraarylmethane-based stopper **6** was obtained (Scheme 1) in 50% yield by a modification of the procedure already reported<sup>10</sup> in the literature. Although we previously used the phenol **6** as its potassium salt during its alkylation, we now prefer to isolate it directly as the phenol after acid-catalyzed reaction between (4-*tert*-butylphenyl)-4-ethylmethanol<sup>10</sup> (**4**) and phenol (**5**). Alkylation of **6** with 2-[2-(2-chloroethoxy)ethoxy]tetrahydropyran<sup>11</sup> (**7**) in *n*-butanol, followed by removal of the THP-protecting group with aqueous HCl gave **8** in 84% yield. The alcohol **8** can either be brominated using CBr<sub>4</sub> and Ph<sub>3</sub>P in CH<sub>2</sub>Cl<sub>2</sub> or tosylated using TsCl in a mixture of THF–H<sub>2</sub>O, affording **9** or **10** in 95 or 53% yields, respectively. Subsequent treatment of **9** or **10** with NaI gave the corresponding iodide **11** in 95% yield or better.

For the synthesis (Scheme 2) of the hydrophilic stopper, we employed a modified literature procedure.<sup>12</sup> Methyl 4-hydroxybenzoate (**12**) was alkylated (K<sub>2</sub>CO<sub>3</sub> in MeCN) with toluene-4-sulfonic acid 2-(2-methoxyethoxy)ethyl ester<sup>13</sup> (**13**). The resulting ester **14** was reduced (LiAlH<sub>4</sub>/THF), and the benzyl alcohol **15** was chlorinated (SOCl<sub>2</sub>/CH<sub>2</sub>Cl<sub>2</sub>), affording **16** in 60% overall yield for the three steps. Alkylation (K<sub>2</sub>CO<sub>3</sub>/DMF) of

**Scheme 1.** Synthesis of the Hydrophobic Stopper.



methyl 3,4,5-trihydroxybenzoate (**17**) with the chloride **16** gave the ester **18** in 82% yield. Compound **20** was isolated in 68% overall yield following (i) reduction (LiAlH<sub>4</sub>/THF) of **18** to give the alcohol **19** and (ii) chlorination (SOCl<sub>2</sub>/DTBMP/CH<sub>2</sub>Cl<sub>2</sub>) of this alcohol. Next, 4-hydroxybenzyl alcohol (**21**) was alkylated (K<sub>2</sub>CO<sub>3</sub>/DMF) with the chloride **20** to yield the alcohol **22**, which was chlorinated (SOCl<sub>2</sub>/DTBMP/CH<sub>2</sub>Cl<sub>2</sub>) in 95%

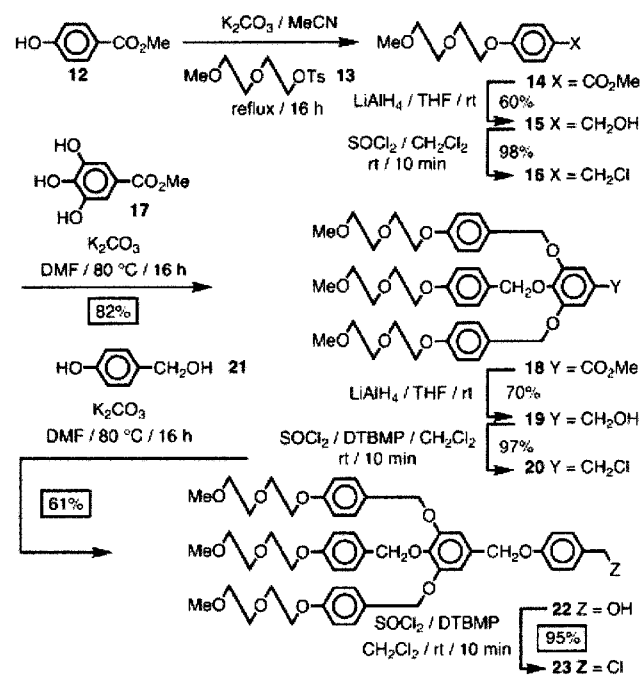
(10) Ashton, P. R.; Ballardini, R.; Belohradsky, M.; Gandolfi, M. T.; Philp, D.; Prodi, L.; Raymo, F. M.; Reddington, M. V.; Spencer, N.; Stoddart, J. F.; Venturi, M.; Williams, D. J. *J. Am. Chem. Soc.* **1996**, *118*, 4931–4951.

(11) Gibson, H. W.; Lee, S.-H.; Engen, P. T.; Lacavalier, P.; Sze, J.; Shen, Y. X.; Bheda, M. *J. Org. Chem.* **1993**, *58*, 3748–3756.

(12) Percec, V.; Cho, W.-D.; Mosier, P. E.; Ungar, G.; Yeardley, D. J. *P. J. Am. Chem. Soc.* **1998**, *120*, 11061–11070 and references therein.

(13) Satoru, I.; Hideo, M.; Kioshi, T. *J. Chem. Soc., Perkin Trans. 1* **1997**, 1357–1360.

## Scheme 2. Synthesis of the Hydrophilic Stopper.



yield to give the hydrophilic stopper as a reactive benzyl chloride **23**.

The synthesis of the [2]rotaxane **3**· $4\text{PF}_6$  is outlined in Scheme 3. A THF–MeOH solution of the asymmetric tetrathiafulvalene (TTF) derivative<sup>14</sup> was treated with 1 equiv of  $\text{CsOH}\cdot\text{H}_2\text{O}$  to generate a TTF–monothiolate which could subsequently be alkylated with 1 equiv of either the bromide **9** or the iodide **11** affording **25** in 76 or 91% yields, respectively. Removal of the tosyl-protecting group from **25** was achieved in 92% yield by refluxing the *N*-tosylate in THF–MeOH containing an excess of NaOMe. Following *N*-alkylation (NaH/DMF) of the pyrrole unit in **26** with the chloride **23**, the dumbbell-shaped compound **27** was isolated in 80% yield. Using this compound as a template for the formation of the cyclobis(paraquat-*p*-phenylene) tetracation in DMF and starting from the dicationic precursor<sup>15</sup> **28**· $2\text{PF}_6$  and 1,4-bis(bromomethyl)benzene (**29**) afforded the single-station [2]rotaxane **3**· $4\text{PF}_6$  in 8% yield.

The synthesis of the semi-dumbbell compound **2**, prior to its being added to cyclobis(paraquat-*p*-phenylene) tetrakis(hexafluorophosphate)<sup>16</sup> **CBPQT**· $4\text{PF}_6$  to form the [2]pseudorotaxane **2**·**CBPQT**<sup>4+</sup> is outlined in Scheme 4. The monotosylate **30**, which was obtained ( $\text{TsCl}/\text{NEt}_3/\text{CH}_2\text{Cl}_2$ ) in 48% yield from 1,5-bis[2-(2-hydroxyethoxy)ethoxy]naphthalene,<sup>17</sup> was converted ( $\text{NaI}/\text{Me}_2\text{CO}$ ) almost quantitatively into the iodide **31** which was protected ( $\text{DHP}/\text{TsOH}/\text{CH}_2\text{Cl}_2$ ) in 88% yield to give the THP “ether” **32**. Alkylation ( $\text{NaH}/\text{DMF}$ ) of compound **26** (Scheme 3) with the iodide **32** afforded in 86% yield the

(14) Jeppesen, J. O.; Takimiya, K.; Jensen, F.; Brimert, K.; Nielsen, K.; Thorup, N.; Becher, J. *J. Org. Chem.* **2000**, *65*, 5794–5805.

(15) Anelli, P.-L.; Ballardini, R.; Balzani, V.; Gandolfi, M. T.; Goodnow, T. T.; Kaifer, A. E.; Pietraszkiewicz, M.; Prodi, L.; Reddington, M. V.; Slawin, A. M. Z.; Spencer, N.; Vicent, C.; Williams, D. J. *J. Am. Chem. Soc.* **1992**, *114*, 193–218.

(16) (a) Odell, B.; Slawin, A. M. Z.; Spencer, N.; Stoddart, J. F.; Williams, D. J. *Angew. Chem., Int. Ed. Engl.* **1988**, *27*, 1547–1551. (b) Asakawa, M.; Dehaen, W.; L’abbé, G.; Menzer, S.; Nouwen, J.; Ramyo, F. M.; Stoddart, J. F.; Williams, D. J. *J. Org. Chem.* **1996**, *61*, 9591–9595.

(17) Ashton, P. R.; Ballardini, R.; Balzani, V.; Boyd, S. E.; Credi, A.; Gandolfi, M. T.; Gómez-López, M.; Iqbal, S.; Philp, D.; Preece, J. A.; Prodi, L.; Ricketts, H. G.; Stoddart, J. F.; Tolley, M. S.; Venturi, M.; White, A. J. P.; Williams, D. J. *Chem. Eur. J.* **1997**, *3*, 152–170.

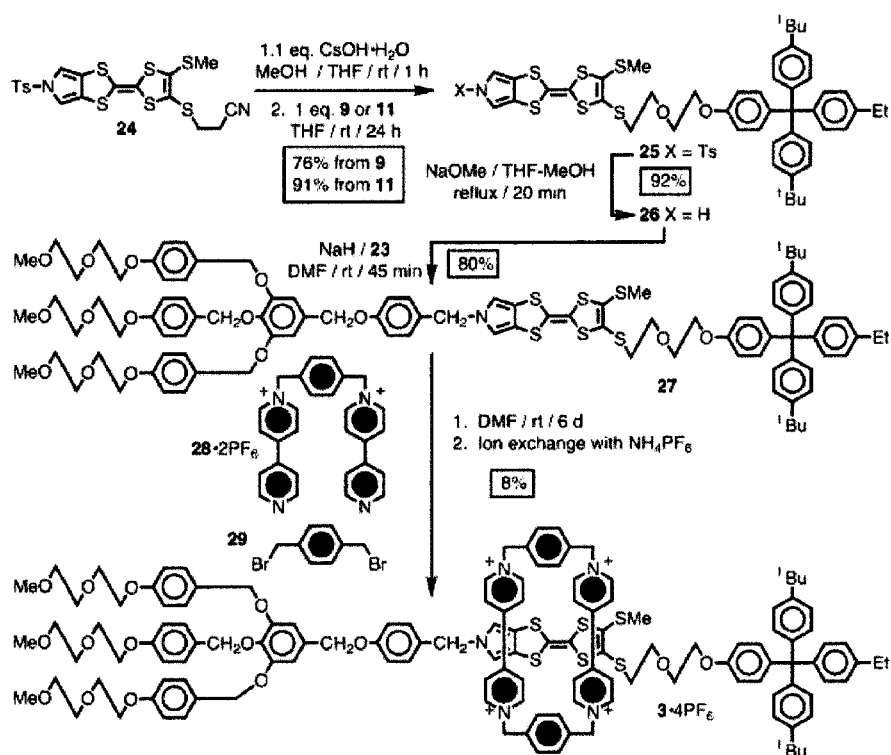
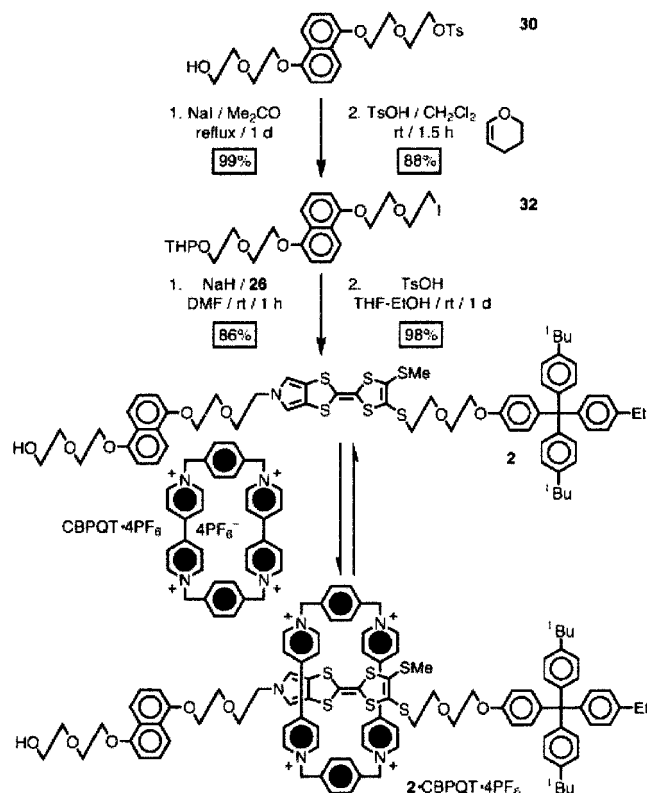
protected semidumbbell compound **33**, which on treatment with TsOH in THF–EtOH, gave the semidumbbell compound **2** in 98% yield.

**Solution-State Characterization.** The full characterization of the [2]catenane and **1**<sup>4+</sup> has already been reported.<sup>8</sup> The [2]-rotaxane **3**<sup>4+</sup> contains only one donor station—the TTF unit—and exhibits a charge transfer (CT) band centered around 810 nm ( $\epsilon = 1400 \text{ L mol}^{-1} \text{ cm}^{-1}$ ) in  $\text{Me}_2\text{CO}$  at 298 K. Since the two-station [2]pseudorotaxane **2**·**CBPQT**<sup>4+</sup> contains two donor units—a TTF unit and a NP one—it is expected to exist as a mixture of two co-conformers—one where the **CBPQT**<sup>4+</sup> encircles the TTF unit and the other where the **CBPQT**<sup>4+</sup> resides around the NP unit. In fact, a 1:1 mixture of **CBPQT**<sup>4+</sup> and the semidumbbell **2** exhibits CT bands centered around 540 nm ( $\epsilon = 870 \text{ L mol}^{-1} \text{ cm}^{-1}$ )—for the NP·**CBPQT**<sup>4+</sup> CT interaction—and 785 nm ( $\epsilon = 1000 \text{ L mol}^{-1} \text{ cm}^{-1}$ ) for the TTF·**CBPQT**<sup>4+</sup> CT interaction in MeCN at 298 K which indicates that the [2]-pseudorotaxane **2**·**CBPQT**<sup>4+</sup> is indeed a mixture of two co-conformers. UV–vis dilution experiments were carried out to determine<sup>18</sup> the binding constant ( $K_a$ ) for 1:1 complexation of **CBPQT**<sup>4+</sup> with the semidumbbell **20**.  $K_a$  Values were obtained using both the NP·**CBPQT**<sup>4+</sup> and TTF·**CBPQT**<sup>4+</sup> CT absorption bands as probes: They were  $85000 \pm 15000$  and  $95000 \pm 15000 \text{ M}^{-1}$ , respectively, corresponding to free energies of complexation of just under  $7 \text{ kcal mol}^{-1}$ .

**Solid-State Device Fabrication.** Solid-state molecular switch tunnel junctions were fabricated from (1) the [2]catenane **1**<sup>4+</sup>, (2) the [2]pseudorotaxane **2**·**CBPQT**<sup>4+</sup>, and (3) the [2]rotaxane **3**<sup>4+</sup> in an effort to elucidate molecular (super)structure/device property relationships. The starting point for all of the devices was (100) Si wafers coated with a thick ( $0.1 \mu\text{m}$ ) oxide ( $\text{SiO}_2$ ) film. All devices were fabricated using optical- or electron-beam lithographically defined n-type polycrystalline (poly-Si) bottom electrodes ( $0.05$  or  $5 \mu\text{m}$  wide and resistivity of  $0.02 \Omega\text{-cm}$ ). Typically, poly-Si films formed via direct chemical vapor deposition growth onto  $\text{SiO}_2$  are neither smooth nor defect free. Since amorphous Si films can be very smooth,<sup>19</sup> however, amorphous Si was used as the starting point for the fabrication of smooth poly-Si electrodes. This many-step process, which has been described previously,<sup>1</sup> was critical for achieving a high (>90%) device yield. Single monolayer films of **1**<sup>4+</sup>, **2**·**CBPQT**<sup>4+</sup>, and **3**<sup>4+</sup> were transferred onto the poly-Si electrode-patterned substrates as Langmuir–Blodgett (LB) films (see below). Following LB film deposition,  $0.05$  or  $10 \mu\text{m}$ -wide top electrodes ( $50 \text{ \AA}$  Ti followed by  $1000 \text{ \AA}$  Al) were deposited onto the LB film using electron-beam evaporation. Except where noted otherwise, devices were measured in air and at room temperature, using a shielded probe station with coaxial probes. Bias voltages were applied to the poly-Si electrode, and the top electrode was connected to ground through a DL Instruments 1211 current preamplifier. For certain experiments, such as device cycling and remnant molecular signature measurements, a series of “write” voltage pulses were applied to perturb the device, and the response was “read” through the current preamp by applying some constant (small) bias. For those measurements, a mechanical relay switch was placed between the device, and the current preamplifier was only connected electrically to the device when the device was actually being “read”. Otherwise, the relay switch connected the device directly to ground.

(18)  $K_a$  values were also obtained for this 1:1 complex in  $\text{Me}_2\text{CO}$  at 298 K. Using the NP·**CBPQT**<sup>4+</sup> and TTF·**CBPQT**<sup>4+</sup> CT absorption bands, centered on 545 nm ( $\epsilon = 760 \text{ L mol}^{-1} \text{ cm}^{-1}$ ) and 745 nm ( $\epsilon = 590 \text{ L mol}^{-1} \text{ cm}^{-1}$ ), respectively, a common value of  $25000 \pm 3000 \text{ M}^{-1}$  was obtained for  $K_a$  corresponding to a free-energy complexation of  $6 \text{ kcal mol}^{-1}$ .

(19) Kamins, T. *Polycrystalline Silicon for Integrated Circuit Applications*; Kluwer Academic: Boston, 1988.

**Scheme 3.** Synthesis of the [2]Rotaxane **3**<sup>4+</sup>**Scheme 4.** Synthesis of the Semidumbbell Compound **2** and the Formation of the [2]Pseudorotaxane **2**·CBPQT<sup>4+</sup>.

Langmuir molecular monolayers of (1) the [2]catenane **1**<sup>4+</sup>, (2) the [2]pseudorotaxane **2**·CBPQT<sup>4+</sup>, and (3) the [2]rotaxane **3**<sup>4+</sup> were prepared on the water surface of a temperature-controlled NIMA Type 611 trough. For all Langmuir films, the compounds were deposited onto the water surface at 20 °C and allowed to equilibrate for 30 min prior to transferring them to the patterned substrates. The subphase was either (a) 18.2 MΩ

H<sub>2</sub>O or (b) 18.2 MΩ H<sub>2</sub>O containing 6.4 mM CdCl<sub>2</sub> (aq), adjusted to pH 8.5 with NaOH (aq). The Langmuir monolayers were compressed at 10 cm<sup>2</sup>/min to a surface pressure of 1.0 mN/m, 5 cm<sup>2</sup>/min to a surface pressure of 14.0 mN/m, and finally at 2 cm<sup>2</sup>/min to the deposition pressure of 30 mN/m. The monolayers were then deposited as LB films onto the electrode-patterned poly-Si substrates on the upstroke at 1 mm/min, after equilibrating for 3 min. Compounds **1**<sup>4+</sup> and **3**<sup>4+</sup> and complex **2**·CBPQT<sup>4+</sup> were transferred as LB monolayers at (supra)molecular areas of 74(5), 83(6), and 38(4) Å<sup>2</sup>/(super)molecule respectively, on an aqueous CdCl<sub>2</sub> subphase, or at 125-(8), 122(8), and 35(4) Å<sup>2</sup>/(super)molecule using a pure water subphase.

The preparation of monolayers of the [2]catenane **1**<sup>4+</sup> has been described previously.<sup>1</sup> The tetracationic compound was co-deposited on the subphase with an anchoring phospholipid, dimyristoylphosphatidic acid, as the counterion (DMPA<sup>-</sup>). The DMPA<sup>-</sup> anion, employed initially as its monosodium salt dissolved in CHCl<sub>3</sub>/MeOH (3:1), and the PF<sub>6</sub><sup>-</sup> salt of the tetracationic [2]catenane were dissolved initially in MeCN. Immediately before spreading, the DMPA and catenane solutions were mixed in a 6:1 molar ratio. By contrast, the amphiphilic [2]rotaxane **3**<sup>4+</sup> was spread directly as its 4PF<sub>6</sub><sup>-</sup> salt from a CHCl<sub>3</sub>/MeCN (20:1) solution. Finally, the [2]pseudorotaxane **2**·CBPQT<sup>4+</sup> is different from the [2]catenane **1**<sup>4+</sup>, and the [2]rotaxane **3**<sup>4+</sup>, insofar as its semidumbbell component, containing the two π-electron rich recognition sites, can dissociate easily from the tetracationic cyclophane (CBPQT<sup>4+</sup>) component. Monolayers of this 1:1 complex were prepared by mixing Na·DMPA, CBPQT<sup>4+</sup>, dissolved initially in MeCN as its 4PF<sub>6</sub><sup>-</sup> salt and the semidumbbell component **2** dissolved in MeCN, in a 12:2:1 molar ratio, prior to spreading.

**Solid-State Device Performance.** There are certain figures of merit that characterize the quality of a two-terminal switching or storage device, and the rank-order of those characteristics is dictated by the targeted application. For these devices, we are concerned with fabricating cross-point memory and logic

structures, meaning that the devices would be arranged in a two-dimensional lattice of crossing wires, similar to an expanded tic-tac-toe board. A disadvantage of the crosspoint architecture is that all devices are electrically interconnected, a feature which implies that the voltages that are used to address (open or close) the devices must be sharp and well-defined. Otherwise, it is very difficult to change the state of one device in the circuit without perturbing neighboring devices—a problem known as “half-select”. Second, it is important to have a large signal difference—resistance or current, for example—between the “open” and “closed” states. Given a sharp address voltage, it is then the magnitude of this signal difference that ultimately dictates the size of the crosspoint structure that can be reliably used. Third, the volatility of the device should be low, since a highly volatile device requires constant refreshing and will correspondingly increase the power consumption and the overhead requirements for operating such a circuit. Fourth, diode—or current rectifying character—of the molecular tunnel junction is an important consideration since diode behavior can lend noise immunity to the various devices within a crosspoint circuit. Such rectification may be either a molecular or an electrode characteristic; this issue, as it relates to molecules, is discussed in some depth below. The final consideration is the switching speed of the device. The fact that speed is the least important consideration is perhaps surprising; indeed, for certain other applications, device-switching speed may be much more vital. However, the cross-point architecture is one that lends itself naturally to parallel addressing, and this factor eases substantially the demands on device-switching speeds.

For all of the devices discussed in this contribution, we carried out measurements that were designed to characterize the sharpness of the address voltages, the magnitude of the switching response, the device volatility, and molecular-dependent current rectification characteristics. The switching speeds of all of the devices arise from a complex interplay of molecular properties and device architecture. Optimization of the switching speed would require an atomic scale engineering of the tunnel barriers that separate the molecules from the electrodes. No such effort was made for this study.

**Structures of the Monolayers.** In this work, it was not just of importance to obtain a uniform coverage of the LB film on the electrode, but it was also necessary to correlate the 2D crystallographic structure of the monolayer with device performance. Therefore, both Langmuir monolayers (on aqueous subphases) and LB (transferred) films were interrogated using Brewster angle microscopy<sup>20</sup> (BAM, Nanofilm Technology). The BAM technique is a polarized light-imaging probe that is sensitive to small changes in the refractive index and can therefore detect structural variations in a molecular monolayer, although, in our case, only to a resolution of approximately 4  $\mu\text{m}^2$ . For certain LB films, smaller features were interrogated using scanning probe microscopy techniques (Digital Instruments SPM).

In Figure 2, BAM images reveal the effects of varying the nature of the subphase on the structure of a Langmuir monolayer and LB monolayer films of the [2]pseudorotaxane. Figure 2a shows characteristic domains indicative of the phase separation of the pure DMPA<sup>-</sup> anions from the mixture of these anions with CBPQT<sup>4+</sup> and the half-dumbbell component **2** of the [2]-pseudorotaxane. Pure DMPA<sup>-</sup> spread on the water subphase under the same conditions (pH and temperature) showed almost identical patterns. Switching to a CdCl<sub>2</sub> (aq) subphase (Figure 2b) resulted in considerably more homogeneous films, at least

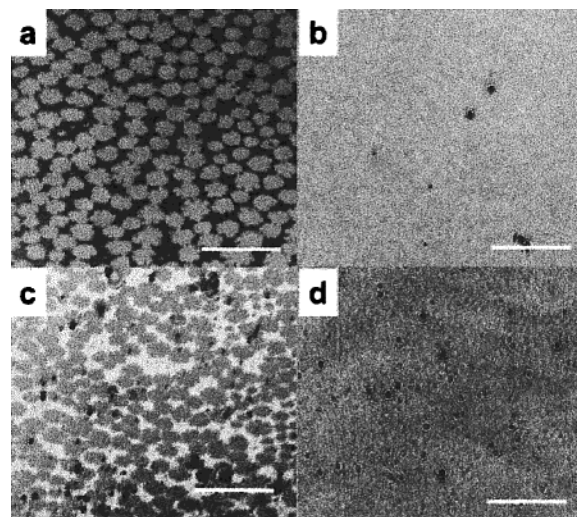


**Figure 2.** BAM images of films of the [2]pseudorotaxane **2**·CBPQT<sup>4+</sup>, taken on different subphases on the Langmuir trough, and as transferred LB films onto glass substrates. (a) Pure water subphase (18.2 M $\Omega$ , pH = 5.5). (b) CdCl<sub>2</sub> (aq) subphase (pH = 8.5). (c) Pure water subphase, transferred to a cleaned glass substrate. (d) CdCl<sub>2</sub> (aq) subphase, transferred to a cleaned glass substrate. The scale bar is 100  $\mu\text{m}$ .

on the length scales accessible with BAM. The divalent Cd<sup>2+</sup> cations have been demonstrated to lessen the electrostatic repulsion between the phospholipid headgroups.<sup>21</sup> This subphase-dependent domain structure was retained in the LB films that were transferred to cleaned glass substrates (Figure 2, c and d), thereby establishing BAM as a structural feedback tool for correlating device performance with monolayer structure. Solid-state devices prepared with the [2]pseudorotaxane transferred from CdCl<sub>2</sub> (aq) subphases, as compared with a pure aqueous subphase, did behave more uniformly from one device to the next. However, even when a CdCl<sub>2</sub> (aq) subphase was utilized, domain formation was still a factor, although the domains were much smaller in size and thus were not resolved by the BAM. The micrometer and submicrometer structures observed for these films are discussed below.

BAM images were also collected from Langmuir monolayers of the [2]catenane **1**<sup>4+</sup> and the [2]rotaxane **3**<sup>4+</sup>. Images of the [2]catenane on pure water versus CdCl<sub>2</sub> (aq) showed, in a similar fashion, the disappearance of structural domains. On the other hand, for the [2]rotaxane, images from Langmuir monolayers formed on pure water and CdCl<sub>2</sub> (aq) appeared similar and featureless. The transport characteristics of the [2]rotaxane-based solid-state devices fabricated with this molecule also did not exhibit a dependence upon subphase. This correspondence appears to highlight the importance of using CdCl<sub>2</sub> (aq) as the subphase when DMPA<sup>-</sup> is used as an anchoring counterion.

Three modes of scanning probe microscopy (SPM), noncontact topographic, lateral contact (friction) force, and surface potential measurements were employed to image the submicrometer structure of LB films transferred onto poly-Si electrodes. Lateral force images revealed structure such as domain boundaries, and this technique exhibited a higher contrast than the noncontact AFM mode. However, only with surface potential imaging were we able to assign chemical identification to the components in the domains. Figure 3 shows simultaneously captured topographic (Figure 3a) and surface potential (Figure 3b) images of a film of **2**·CBPQT·4DMPA transferred onto poly-Si from a CdCl<sub>2</sub> (aq) subphase. Whereas the BAM image

(20) Mobius, D. *Curr. Opin. Colloid Interface. Sci.* **1998**, *3*, 137–142.

(21) Losche, M.; Mohwald, H. *J. Colloid Interface Sci.* **1989**, *131*, 56–67.

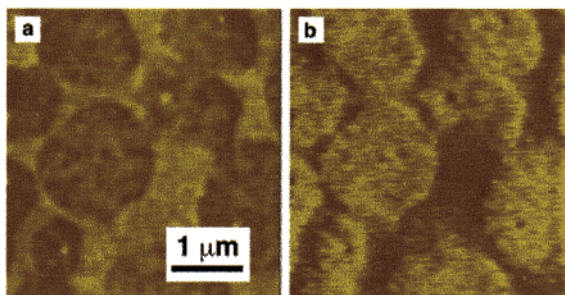


**Figure 3.** “Tapping mode” topographic (a) and surface potential (b) SPM images of an LB film prepared as a Langmuir monolayer on a  $\text{CdCl}_2$  (aq) subphase with a composition of [2]pseudorotaxane  $2\cdot\text{CBPQT}^{4+}/6\text{DMPA}^-/2\text{Na}^+$  and transferred to a poly-Si substrate. BAM images of this film were featureless, as the domain structure is finer-grained than the imaging resolution of the BAM. The surface potential measurements indicate that the circular domains are rich in the [2]pseudorotaxane component, while the topographic measurements indicate some aggregation within the (bright)  $\text{DMPA}^-$ -rich regions.

appeared to be homogeneous, the SPM images revealed that domain structure was still present in this film, although at much smaller length scales than was observed for the pure water subphase.

To measure the surface potential, an oscillating voltage,  $V_{\text{ac}} \sin \omega t$ , was applied directly to the cantilever tip, and this created an oscillating electric force at frequency  $\omega$ . This oscillating force has the amplitude  $F = dC/dz \Delta V_{\text{dc}} V_{\text{ac}}$ , where  $dC/dz$  is the vertical derivative of the tip–sample capacitance,  $\Delta V_{\text{dc}} = V_{\text{tip}} - V_{\text{sample}}$  is the dc voltage difference between the tip and the sample, and  $V_{\text{ac}}$  is the oscillating voltage applied to the tip. When the tip and sample surface are at the same dc potential, the cantilever feels no oscillating force; in surface potential mode, the microscope adjusts the voltage on the tip until the oscillating force on the cantilever vanishes. The tip voltage is then equal to the effective surface potential.

The surface potential measured this way is directly proportional to the density of dipole moments directed perpendicular to the surface.<sup>22</sup> Thus, bright areas in the surface potential image correspond to a higher density of vertically directed dipole moments. A component of the film that is richer in the [2]pseudorotaxane will possess a higher dipole density than a component richer in phospholipid ( $\text{DMPA}^-$ ) counterion. Therefore, the bright areas in the surface potential image correspond to a domain that is at least dominated by the [2]pseudorotaxane. The corresponding topographic image shows these regions to be dark, with a height difference of about 5 nm between the bright and dark regions. This observation implies that the component rich in  $\text{DMPA}^-$  is aggregating or polymerizing, and this result can be corroborated with surface pressure/area isotherms from the Langmuir trough. A film of the [2]pseudorotaxane using a freshly prepared solution of  $\text{Na}\cdot\text{DMPA}$  yielded a lower molecular area ( $\text{\AA}^2/\text{molecule}$ ) at a particular target pressure during transfer than an older  $\text{Na}\cdot\text{DMPA}$  solution. Nevertheless, it was not possible to remove this heterogeneity completely from these films, and some amount of microscopic phase segregation was observed for every [2]pseudorotaxane/ $\text{DMPA}$  LB film. Topographic images of a film of the [2]pseudorotaxane using “fresh”  $\text{Na}\cdot\text{DMPA}$  did reveal a greater uniformity in the structural features of the film, and the height difference between the phase-segregated domains was reduced to about 2 nm.

**The Switching Characteristics of Molecular Electronic Tunnel Junction Devices.** In the case of the devices fabricated

from  $1^{4+}$ ,  $2\cdot\text{CBPQT}^{4+}$ , and  $3^{4+}$ , we expected to observe some switching in the solid-state devices. The general *solution-phase* mechanism for all three molecules is very similar, and we discuss this picture first before moving to the solid-state devices. In the ground state of the molecule (supermolecule), the tetracationic cyclophane encircles the TTF binding site, although for the [2]pseudorotaxane, there is competition between the TTF and NP sites, as discussed above. For all three systems, the first oxidation of the molecule (or complex) corresponds to the removal of an electron from the TTF site, leading to Coulombic repulsion between the  $\text{TTF}^{\bullet+}$  site and the positive charged  $\text{CBPQT}^{4+}$  ring. The [2]catenane  $1^{2+}$  and the [2]pseudorotaxane  $2\cdot\text{CBPQT}^{4+}$  are both bistable systems since both the TTF and the 1,5-dioxynaphthalene (DN) unit can serve as an electron donors. Thus, in those systems, molecular mechanical motion (circumrotation of the crown ether in  $1^{4+}$  and translation of the cyclophane in  $2\cdot\text{CBPQT}^{4+}$ ) is the observed solution-phase switching mechanism. However, in the case of the [2]rotaxane  $3^{4+}$ , the dumbbell component contains only one binding site. Therefore, while oxidation of the TTF unit should induce a small amount of motion on the part of the  $\text{CBPQT}^{4+}$  ring, the switching characteristics of this molecule are expected to be poor relative to either  $1^{4+}$  or  $2\cdot\text{CBPQT}^{4+}$ . When the TTF unit is reduced back to the charge-neutral state, the molecule (supermolecule) will revert back to its ground-state co-conformer on a time-scale that varies from milliseconds to a few seconds, depending on the system.

We previously reported on the characteristics [2]catenane  $1^{4+}$ -based solid-state devices, and we briefly review and expand upon those results here. The [2]catenane devices were stable switches, exhibiting roughly a factor of 100% change in junction resistance between the 0 and 1 states, and could be cycled at least a few hundred times. Moreover, the voltages required to open or close the switches were stable from one cycle to the next and from device-to-device. Monostable [2]catenane control devices (two DN groups in the crown ether ring, rather than one DN and one TTF group), as well as other controls, did exhibit a switching response. The mechanism for the bistable [2]catenane had at least one thermally activated component, and no switching response was observed at temperatures below 230 K. In addition, as the device was cooled stepwise from 330 K to 230 K, the voltages required to open or close the switch systematically increased in amplitude. This was understood as follows: In a single-molecule thick-tunnel junction, when the molecule is oxidized, that charge is balanced by image charges in the electrodes. At lower temperatures, the polysilicon electrode becomes less polarizable and therefore less able to support an image charge. These results taken together implied that at least some critical aspect of the solution-phase redox-activated switching mechanism was retained in the solid-state device.

There were also certain obvious differences between the solution-phase and solid-state switching mechanism, and our previous report<sup>1</sup> on the [2]catenane  $1^{4+}$  highlighted some of those differences. In particular, for both the switch-open and switch-closed states of the device, the TTF group is charge-neutral. Oxidation of the TTF group of the ground (switch-open) state co-conformer does activate circumrotation of the ring and thereby conversion of the device to the switch-closed state. However, in a conducting-tunnel junction, the junction does not remain charged after the bias is removed. For the solid-state device, circumrotation of the crown ether ring back to the ground-state co-conformation is greatly accelerated (by a factor of  $10^3$ ) by applying a reducing bias to the device. One possibility

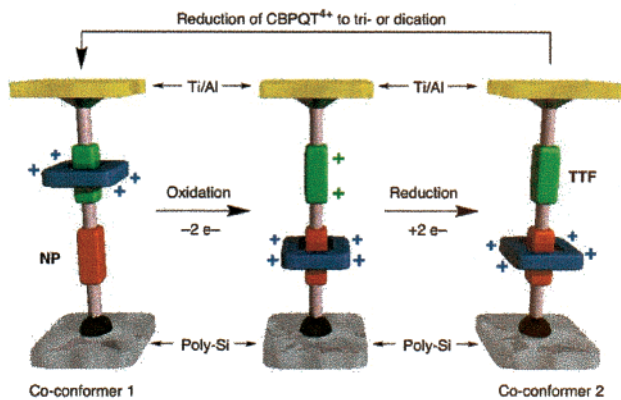


**Figure 4.** This graphical representation depicts a molecular mechanism that is consistent with the observed voltage cycling of the [2]-pseudorotaxane-based solid-state devices. It is not clear which co-conformer represents the ground (switch-open) state of the device and which represents the metastable (switch-closed) state. However, note that it is necessary to charge the dumbbell component (oxidation to go forward, reduction for the reverse pathway) to cycle the device between the two (dumbbell charge neutral) co-conformers.

is that the activation barrier for circumrotation back to the lowest-energy co-conformer is lowered by a partial reduction of the anchoring DMPA $^-$  counterions. As discussed below, a similar phenomena is observed for the 2•CBPQT $^{4+}$  device, and here again, translation of the cyclophane ring from the DN site to the TTF site may be aided by partial reduction of the cyclophane ring. Previously, we proposed a possible mechanism for the [2]catenane  $1^{4+}$  device. In Figure 4, we present a switching mechanism for the 2•CBPQT $^{4+}$  device that is analogous to what we hypothesized for the [2]catenane  $1^{4+}$  device.<sup>1</sup> Note that both the open and closed states of the dumbbell component of the molecular tunnel junction switch are charge neutral, but that the pathways between the two states involve charging the dumbbell component. For the 2•CBPQT $^{4+}$  device, one of the two co-conformers will obviously be the ground state, while the other will be metastable. The reduction of the CBPQT $^{4+}$  ring is a component of the switch-cycling mechanism that is not observed in the solution phase for any of these systems. Other substantial variations between the solid-state and solution-phase switching mechanisms are also likely. For example, interactions between the molecular monolayers and the electrodes may modify the relative stabilities of the various co-conformers. One potentially significant issue is the interaction between the molecular monolayer and the evaporated Ti top electrode material. However, we have previously reported measurements on a number of control molecules, including simple linear-alkyl amphiphiles,<sup>23</sup> as well as the monostable [2]-catenane mentioned above, and others. If the Ti/molecular interface impacts device performance, then that effect is subtle and is not readily observed in the control experiments. In addition, the crystallographic packing of the LB monolayers, as discussed above, will also impact the solid-state device characteristics.

The signature of molecular switching in a (two-terminal) molecular electronic tunnel junction is a hysteretic response in the current–voltage characteristics. Device capacitance actually provides a more general mechanism for generating a hysteretic current/voltage response, since separating charge across a tunnel junction will lead to a dc voltage offset, thereby shifting the

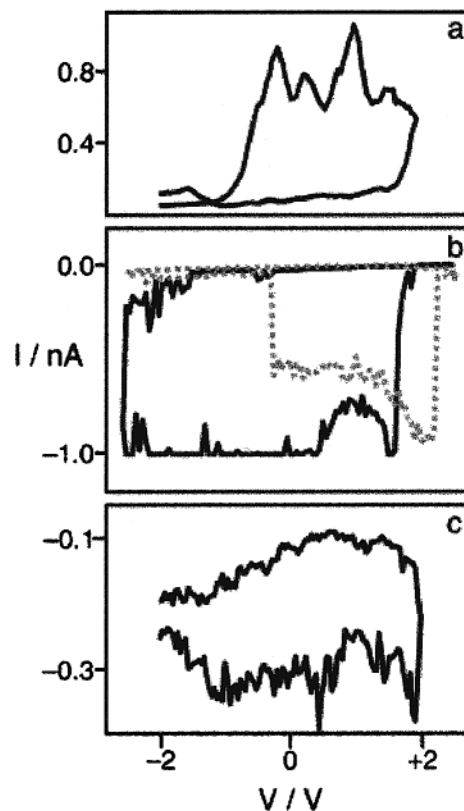


**Figure 5.** Remnant molecular signatures of (a) the [2]catenane  $1^{4+}$ , (b) the [2]pseudorotaxane 2•CBPQT $^{4+}$ , and (c) the [2]rotaxane  $3^{4+}$ . The [2]catenane and the [2]rotaxane devices yielded reproducible curves from experiment-to-experiment, and from device-to-device. The [2]-pseudorotaxane devices, however, exhibited large-amplitude switching signatures that fluctuated from measurement-to-measurement, and two representative measurements are plotted. The remnant molecular signatures were monitored at  $-0.1$  V,  $+0.1$  V, and  $+0.2$  V for molecules  $1^{4+}$ , 2•CBPQT $^{4+}$ , and  $3^{4+}$  respectively.

current–voltage trace by some amount. In fact, such a voltage offset is the signature of charge storage in a junction. However, we are not looking to construct capacitors, but rather molecular switch tunnel junctions. Therefore, to make certain that any observed hysteretic response did not originate from device capacitance, careful measurements, at a resolution of 10 mV and 10–100 pA, were made to ascertain that the current passed from a negative to a positive value at zero-bias. In any event, the actual hysteresis characteristics (switching voltage/switching magnitude) of a device are quantified using a measurement that we have described previously<sup>1</sup> as a remnant molecular signature (RMOs). This experiment, which is similar to the remnant polarization measurement used for ferroelectrics,<sup>24</sup> consists of applying a series of probe and read voltage pulses so that the probe voltages cycle through a loop (from  $-2.5$  to  $+2.5$  V, and back again, for example), and the read voltage is some voltage near zero bias ( $+0.2$  V for example). In this way, the response of the device to some series of applied voltage is interrogated in a relatively nonperturbing fashion, and device capacitance is largely canceled out.

The RMOs curves for the [2]catenane  $1^{4+}$ , the [2]pseudorotaxane 2•CBPQT $^{4+}$ , and the [2]rotaxane  $3^{4+}$  are presented in Figure 5, a, b, and c, respectively. For the [2]pseudorotaxane device we measured the remnant molecular signature curves as a function of the time spent writing to the device (not shown).

(23) Collier, C. P.; Wong, E. W.; Belohradsky, M.; Raymo, F. J.; Stoddart, J. F.; Kuekes, P. J.; Williams, R. S.; Heath, J. R. *Science* **1999**, *285*, 391–394.

(24) Lines, M. E.; Glass, A. M. *Properties and Applications of Ferroelectrics and Related Materials*; Clarendon: Oxford, 1977.

The experiment roughly corresponds to a measurement of the device switching speed. We found that the device could operate from 0.1 to 100 Hz. It is clearly a slow device, exhibiting a collapsing RMolS trace for the faster measurements. Note that if capacitance were responsible for this hysteresis loop, then the RMolS traces would be expected to broaden at faster times. In any case, a simple calculation, based on the amount of current that flows through the device, reveals that the nature of this limitation is likely a combination of molecular properties and device construction. Our 100 Hz (and slower) pseudorotaxane device was about  $5 \mu\text{m} \times 10 \mu\text{m}$  in size, and based on the Langmuir isotherm measurements, contained about  $5 \times 10^6$  molecules. At the voltage required to close the device (around +1.7 V), the current level through the “switch-open” device is approximately 10 nA. At 100 Hz device cycling, only about 1% of the electrons that actually pass through the device cause device switching. Thus, if every electron event resulted in oxidation of the TTF unit and translation of the cyclophane ring, the device could only be operated at about 10 kHz. In a molecular switch tunnel junction device, the current flow through the device, as well as the residence time of a charge on a molecule, is largely limited by the widths and energy heights of the tunnel barriers that separate the redox center of the molecule from the electrodes, although molecular relaxation may also contribute. The probability that a charging event will lead to translation of the cyclophane ring, or, in the case of the [2]catenane, to circumrotation of the crown ether ring, is limited by a combination of electron tunneling rates and molecular properties, such as the activation barrier to ring translation or circumrotation. For the [2]pseudorotaxane device, that product probability is about 1%. Separating the molecular switching properties from the device architecture remains an existing experimental challenge.

The two (gray and black) RMolS traces (Figure 5b) for a device made from  $2\cdot\text{CBPQT}^{4+}$ , the two-station [2]pseudorotaxane, reveal a much more dramatic response than that obtained for the [2]catenane  $3^{4+}$  (Figure 5a). The switching voltages are very sharp and are accompanied by a large magnitude change in current through the device. Repeated RMolS measurements of this and other [2]pseudorotaxane devices consistently reproduced the large current change upon switching. However, while this molecular switch tunnel junction always closed at a positive bias and opened at a negative bias, the actual voltages required for switching the devices fluctuated from experiment-to-experiment. We attribute this phenomenon to the above-discussed domain structure of the supramolecular monolayer. Relative molecular motion in a tightly packed monolayer, such as the translation of the cyclophane ring, is likely to be accompanied by a reorganization of the monolayer. Thus, the switching characteristics of this device are dominated by both the relative motions of individual components of the [2]pseudorotaxane, and also by the reorganization of the supramolecular domains. Domain switching will be accompanied by the statistical fluctuations that accompany any nucleation phenomenon, and is clearly not a desirable characteristic in a molecular switch tunnel junction device.

The RMolS trace (Figure 5c) for a device made from  $3^{4+}$ , the single-station [2]rotaxane, reveals only a very weak switching signature, but one that was highly reproducible from device-to-device. However, even this minimal switching response was only observed for a few device cycles, after which the RMolS trace collapsed. This compound represents our first attempt synthetically at removing domain switching from the device by rendering the [2]rotaxane amphiphilic through the incorporation

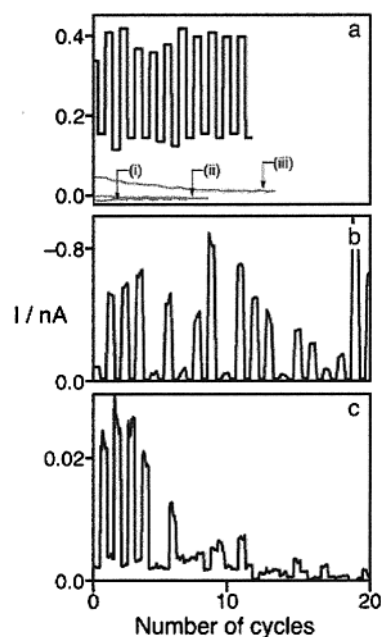


**Figure 6.** Device cycling for (a) the [2]catenane  $1^{4+}$ , (b) the [2]pseudorotaxane  $2\cdot\text{CBPQT}^{4+}$ , and (c) the [2]rotaxane  $3^{4+}$ . Figure 5a also shows control experiments for the bistable [2]catenane·DMPA layer performed by substituting: (i) DMPA as its monosodium salt, (ii) the tetracationic cyclophane  $\text{CBPQT}^{4+}$  anchored with DMPA, and (iii) a singly stable degenerate [2]catenane ( $\text{CBPQT}^{4+}$  interlocking bisparaphenylene[34]crown-10) anchored with DMPA.

of a bulky dendritic hydrophilic stopper—along with a hydrophobic stopper—onto the dumbbell component, thereby increasing the area/molecule in the device. However, the single-station character of the backbone also makes this device effectively a control experiment.

**Device Cycling and Volatility.** The RMolS traces yielded information that could then be used to cycle the devices between the switch-open and switch-closed states, such as the voltages that can open or close a device as well as nonperturbing voltage levels that can be utilized to interrogate the device. In device cycling experiments, voltages of sufficient magnitude to either close or open the molecular switch are applied and, after each application of such a voltage, the state of the device is read at some small, nonperturbing voltage. In Figure 6a-c we present device cycling results for  $1^{4+}$ ,  $2\cdot\text{CBPQT}^{4+}$ , and  $3^{4+}$ , respectively. Device cycling of the [2]catenane  $1^{4+}$  has been reported previously.<sup>1</sup> Its cycling behavior was robust, exhibiting a consistent on/off ratio of approximately 2–3 for a few hundred cycles, and it could be repeatedly sampled over a period of about 2 months. Included with the results for  $1^{4+}$  (Figure 6a) are control experiments performed by substituting the components described in the Figure caption for the bistable [2]catenane/DMPA film in the devices. Although a very small amount of switching (<1% of the  $1^{4+}$  bistable [2]catenane device) was observed for the DMPA film, such switching was attributable to a small amount of device capacitance, as measured by a nonzero current at zero applied bias. Bistability was not observed in a RMolS trace for this control.

The current/voltage traces for devices made from the [2]pseudorotaxane  $2\cdot\text{CBPQT}^{4+}$  were consistent with the RMolS traces in which a large amplitude molecular switching signal was apparently strongly coupled with the domain fluctuations in the 2D film. For the device cycling experiments, the change in current signal through this device was higher than  $10^2$  for some cycles, but cycle-to-cycle reproducibility was poor. The single-station [2] rotaxane  $3^{4+}$  exhibited reasonably stable, but

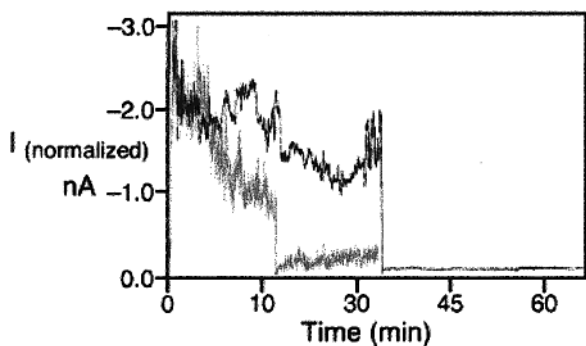


**Figure 7.** The temporal stability of the “closed” and “open” states of molecular switch tunnel junctions fabricated from  $1^{4+}$  (gray) and  $2\cdot\text{CBPQT}^{4+}$  (black).

low-amplitude, switching characteristics for very few cycles, after which the performance of this device degraded rapidly—consistent with the RMoS measurements on this device. The origin of this switching is not clear. Two possibilities are the redox-driven translation of the cyclophane off of the TTF site or field-driven reorganization of the molecular components. However, the small amount of switching that did occur did not arise from device capacitance.

The two best molecular switch tunnel junctions reported here—those made from  $1^{4+}$  and  $2\cdot\text{CBPQT}^{4+}$ —exhibit reasonably good volatility characteristics. Devices made from  $3^{4+}$  relaxed from the switch-closed state within a couple of minutes, consistent with the picture that true bistability does not exist in this device. In Figure 7, we present volatility measurements for both the [2]catenane- and [2]pseudorotaxane-based devices. In these experiments, the devices were initially set to the “switch closed” state by applying a voltage of +2 V for a couple of seconds, and then the current through the devices was monitored for 1000 or 2000 s, respectively. Applying a bias of -2 V for a few seconds then opened the device, and the current was monitored again. The switch-closed state  $1/e$  decay times of the [2]catenane and the [2]pseudorotaxane-based devices were 20 and 60 min, respectively, while the switch-open states for both devices did not exhibit a time dependence. For the [2]pseudorotaxane device, the switch-closed state is substantially noisier than the switch-open state, and sudden jumps in the current through the device were recorded as a function of time. We believe that this erratic behavior is, once again, a signature of domain switching. In all of the devices that we have measured, the switch-open state represents the initial state of the device and likely represents the ground state of the molecule or supermolecule. The excited-state co-conformation of both  $1^{4+}$  and  $2\cdot\text{CBPQT}^{4+}$  represents a molecular structure or superstructure with a narrower HOMO–LUMO gap. Such a gap translates into a higher density of states in the molecular tunnel junction of the solid-state device and, in principle, higher current flow through the device. The finite volatility of the switch-closed states of these devices is consistent with this picture.

**Diode Behavior and its Molecular Origins.** One of the earliest suggestions for a molecular electronic device was Aviram and Ratner’s proposal<sup>25</sup> for a molecular rectifier, based on a molecular electron donor/acceptor complex that bridges across two electrodes. If the donor and the acceptor portions of the complex are well separated between the electrodes, then current flow in the acceptor to donor direction encounters less resistance than the current flow in the opposite direction. This

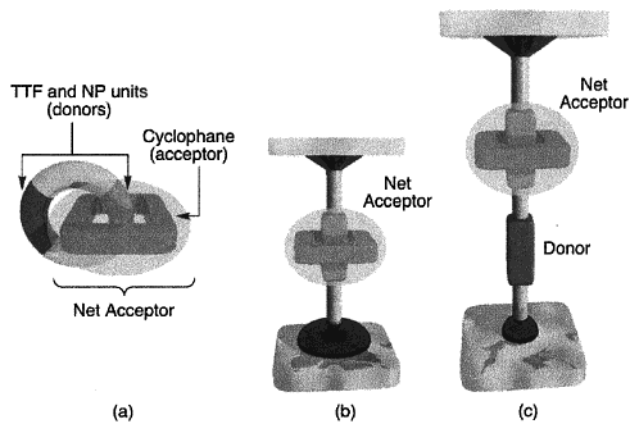


**Figure 8.** The different molecular architectures [(a) the [2]catenane, (b) the [2]rotaxane, and (c) the [2]pseudorotaxane] within the context of a donor/acceptor picture for the molecular switch tunnel junctions. The gray shaded area represents the “net” acceptor site on the (super)molecule, where the tetracationic cyclophane encircles one of the  $\pi$ -electron rich stations.

prediction has been verified<sup>26,27</sup> experimentally. Current rectification does, in fact, appear to be a device characteristic that is under synthetic control at the molecular level. The molecules and supermolecule discussed here are all based on donor–acceptor complexes and units. Hence, it is instructive to analyze the  $I/V$  characteristics of these devices in the context of donor and acceptor units.

For the purpose of this discussion, we will consider the TTF unit and 1,5-dioxynaphthalene ring system in  $1^{4+}$ ,  $2\cdot\text{CBPQT}^{4+}$  and  $3^{4+}$  as electron donors of varying strengths and the bipyridinium units of  $\text{CBPQT}^{4+}$  as electron acceptors. Within this context, it is possible that when the tetracationic cyclophane binds with one of the donor sites, and then the entire recognition center becomes a “net” acceptor site. Thus, we can view the [2]catenane, the [2]pseudorotaxane, and the [2]rotaxane as the rather idealized entities shown in Figure 8.

In Figure 9, we plot the current–voltage ( $I/V$ ) traces of all three devices for both the switch-closed and the switch-open states. To highlight the rectifying character of these devices, we have expanded these traces near the region of zero-bias. The first thing to note is that—as discussed in the previous section—all traces cross zero-current at zero-bias, indicating that capacitance effects are not being measured here. Second, while the various data discussed earlier—such as the RMoS traces, exhibited some variation from sample to sample, it is the  $I/V$  traces that appear to be the most sensitive to the molecular variations from device-to-device. The third common feature is that all devices, in their switch-closed states, exhibit higher current flow at both negative and positive bias. This observation is consistent with the proposed model in which the excited-state co-conformer of these (super)molecules has a higher density of states and is therefore a generally better conductor.

The  $I/V$  traces (Figure 9a) for the [2]catenane reveal a slight diode effect at positive bias for both the switch-closed and switch-open states. Although this molecule is made up of interlocked donor and acceptor portions, it does not meet the criterion of having the donor and acceptor portions well-separated in the path between the electrodes. In fact, the actual geometry of this device is such that the entire [2]catenane is located at the poly-Si end of the molecular junction, while the phospholipid ( $\text{DMPA}^-$ ) anions sit on top of the [2]catenane and

(25) Aviram, A.; Ratner, M. R. *Chem. Phys. Lett.* **1974**, *29*, 277–283.

(26) Metzger, R. M. *Acc. Chem. Res.* **1999**, *32*, 950–957.

(27) Metzger, R. M. *J. Mater. Chem.* **2000**, *10*, 55–62.

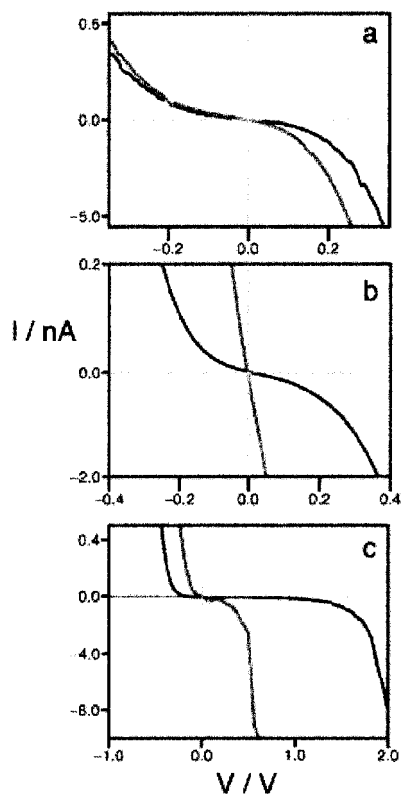


**Figure 9.** Current–voltage traces of the three molecular switch tunnel junction devices: (a) the [2]catenane  $1^{4+}$ , (b) the [2]rotaxane  $3^{4+}$ , and (c) the [2]pseudorotaxane  $2 \cdot \text{CBPQT}^{4+}$ . The gray curves are the switch “closed” configuration, while the black curves are the switch “open” configuration, and represent the initial state of the device.

contact the top Ti/Al electrode. Thus, we conclude that the slight asymmetry of these  $I/V$  curves arises largely from the asymmetric architecture of the molecular junction, rather than from a donor–acceptor interaction.

The single-station [2]rotaxane  $3^{4+}$  is simply an acceptor separated by the electrodes at the hydrophilic and hydrophobic ends of the molecule. This molecular junction should exhibit the most symmetric  $I/V$  responses of all the devices discussed here, and indeed, in both the switch-closed and in the switch-open state, the response (Figure 9b) is quite symmetric about zero-bias. Control experiments using amphiphilic long chain alkanes were carried out in order to quantify any rectification behavior that arose from just the asymmetric nature of the metal/insulator/semiconductor junction. A small amount of asymmetry in the current/voltage trace was observed, and it nearly exactly maps onto the asymmetry of the [2]rotaxane  $3^{4+}$  device.

Finally, the most revealing of these  $I/V$  traces (Figure 9c) is that of the two station [2]pseudorotaxane  $2 \cdot \text{CBPQT}^{4+}$ . This device exhibits particularly strong current rectification properties in the switch-open, positive-bias mode. In this bias, electrons are flowing from the Ti/Al electrode, through the supermolecule, and into the poly-Si electrode. According to the model of Aviram and Ratner,<sup>25</sup> this measurement implies that the ground (switch-open) state of the pseudorotaxane is the co-conformer that has the CBPQT<sup>4+</sup> ring associated with the 1,5-dioxynaphthalene site. When the switch is closed, the junction becomes conducting at either bias. On the basis of the donor–acceptor argument, one might expect some current rectification at a negative bias in the switch-closed state, but no such rectification is observed. In fact, at negative bias voltages below a few tenths of a volt, the conductance ( $dI/dV$ ) (but not the current magnitude) of both the switch-closed and switch-open states is actually quite

similar. One explanation is that only a fraction of the [2]-pseudorotaxane domains are actually switching. Given that domain fluctuations are certainly key to understanding the performance of this device, this possibility is not unlikely. Nevertheless, the current–voltage traces presented here were highly reproducible from device-to-device. Although the donor–acceptor picture does provide some insight, it is probably not the complete story. Other experiments, however, such as exploring different donor sites and extending the physical separation between the donor sites in a rotaxane or pseudorotaxane (supra)molecular architecture, are suggested by these results.

## Conclusions

Solid-state molecular tunnel junction switching devices were fabricated by sandwiching LB monolayers of a bistable [2]-catenane, a bistable [2]pseudorotaxane, and a single-station [2]-rotaxane between an n-type polySilicon bottom electrode (adjacent to the hydrophilic end of the LB film) and a titanium/aluminum top electrode. The electrical properties were found to be highly dependent on supramolecular structure, the presence of bistability within the (super)molecule, and the crystallographic organization of the LB film. The [2]catenane-based devices exhibited stable operation over many device cycles, but with only a relatively small conductance change (factor of 2–3) between the switch-open and switch-closed states. Large conductance changes ( $10^2$ ) between the switch-closed and the switch-open states could be observed for the [2]pseudorotaxane-based device, but the overall characteristics of that device were complicated by the presence of molecular domains within the LB film. The single-station [2]rotaxane was designed with a bulky, hydrophilic stopper, so as to generate a large area/molecule, and therefore to avoid the complexities of domain switching. While domain switching was not observed for those devices, the general performance characteristics of those devices were poor. This result was not unexpected since bistability was not incorporated into the design of the [2]rotaxane molecule.

The current/voltage characteristics of these devices were considered within the framework of a donor acceptor model. This model provides a reasonably consistent framework for understanding these switching devices. It also suggested a number of new target molecular switch architectures.

This paper represents a significant first step toward elucidating molecular structure/device property relationships for active molecular electronics devices.

## Experimental Section

Full experimental details and compound characterizations along with electrode fabrication and monolayer formation protocols are provided in the Supporting Information.

**Acknowledgment.** This work was funded by the Defense Advanced Research Projects Agency, the Semiconductor Research Corporation, and the Office of Naval Research. C.P.C. is an employee of the Hewlett-Packard Corporation, and the NMR spectrometer used in this work was supported by the National Science Foundation. We thank the University of Odense for a Ph.D. Scholarship to J.O.J..

**Supporting Information Available:** Full experimental details and compound characterizations; also, electrode fabrication and monolayer formation protocols (PDF). This material is available free of charge via the Internet at <http://pubs.acs.org>.